*[Handwritten annotations at top:]*
*(M1) repetition of information to clear out! 22, 23*
*1/ lines 15 St Hey    4/ data reduction 21, 24*
*2/ target (X1, X2    5/ pol-cal 41, 42*
*3/ date    41, 42    6/ wave V1, V2*
*7/ line list 47, 24 order*
*8/ HAZEL N1, N2, N3 capital? All!*

*[Handwritten: (M2) messy...! Va very bad! structure layout with SCHEDULE !!]*

# Dynamic Jet-like event in the AR with a C-class flare and its spectacular profiles

Z. VASHALOMIDZE,[1,2,3] T.V. ZAQARASHVILI,[4,2,3] M. BENKO,[1] D. KURIDZE,[5] P. GÖMÖRY,[1] J. RYBÁK,[1] AND M. COLLADOS[6,7]

[1] Astronomical Institute, Slovak Academy of Sciences
05960 Tatranská Lomnica, Slovak Republic
[2] Evgeni Kharadze Georgian National Astrophysical Observatory,
Mount Kanobili, 0301 Abastumani, Georgia
[3] Space Research Center, Ilia State University,
Kakutsa Cholokashvili Ave 3/5, 0162 Tbilisi, Georgia
[4] IGAM, Institute of Physics, University of Graz
Universitätsplatz 5, 8010 Graz, Austria
[5] National Solar Observatory
3665 Discovery Drive, Boulder, CO 80303, USA
[6] Instituto de Astrofísica de Canarias (IAC)
E-38205 La Laguna, Tenerife, Spain
[7] Departamento de Astrofísica, Universidad de La Laguna
E-38206 La Laguna, Tenerife, Spain

*[Handwritten: (M3) Minimize would no introduction that]*
*[Handwritten: (M4) coalignment → coordinate units!]*

## ABSTRACT

The influence of solar flares on the dynamics of lower atmospheric plasma is not yet fully understood. We performed full-Stokes spectro-polarimetric observations of active region NOAA 3363 on GREGOR Infrared Spectrograph (GRIS) during consecutive C-class flares on July 16, 2023. The near-infrared spectral interval covered photospheric Si I 10827 Å and Ca I 10839 Å lines and chromospheric He I 10830 Å triplet line. Besides the enhanced emission of He I 10830 Å triplet, the upper photospheric line Si I 10827 Å also showed a significant increase in intensity. The intensity of the Si I line was increased after several minutes of He I enhancement, which indicates slow energy transfer from the chromosphere to the upper photosphere. We speculate that the heat transfer by thermal conduction from the formation height of He I to the formation height of Si I line is responsible for the observed time delay.

*Keywords:* Sun: chromosphere – Sun: flares – Sun: magnetic fields – Sun: photosphere – techniques: polarimetric

*[Handwritten margin: of → the]*
*[Handwritten under text: the ; the]*
*[Handwritten circled right margin: the ... at 104 ... ?]*

## 1. INTRODUCTION

For many years, researchers have examined collimated ejections of chromospheric plasma into the corona. Jets are essential building blocks of the solar chromosphere. Spicules and mottles constitute the main features of the chromospheric jets (Beckers (1968), De Pontieu et al. (2007), van der Voort et al. (2009), Moore et al. (2011), Tsiropoula & Suematsu (2012), Sterling et al. (2020)). Surges, on the other hand, are chromospheric jets that appear dark in Hα images and can reach heights of up to 200 Mm (Roy (1973); Yoshimura et al. (2003)). Recent studies have also identified small chromospheric jets with loop structures at their bases (Shibata et al. (2007)).

Flares, high-speed reconnection jets and coronal mass ejections characterized by sudden releases of magnetic energy originate from changes in the magnetic field structure in the corona. High energy particles, accelerated during the flare, penetrate the lower regions and heat the local plasma through interaction with atoms. This leads to the enhanced emission of chromospheric plasma. During the intense flares, the photosphere responds to the flaring event with increased emission (while light flares). However, it is difficult to determine the penetration height of flare-related particles.

Spectral lines, such as the He I 10830 Å triplet, formed in the chromosphere may give valuable information about the potential impact on the surrounding environment. Observations of this line, along with other diagnostic lines like

*[Handwritten annotations in bottom margins:]*
*of → the*
*other words*
*of what*
*2)   Add something on solar quakes - sunquakes - Kosovichev.*
*+ B   high-Jed*
*Some double example 1: (1) GRIS - profiles → jet → HAZEL modeling*
*(2) = DO AIA + HMI + GOES flares*
*(3) jet ~ flares*
*citation citations*

the Si I 10827 Å line, provide valuable information about the temperature and dynamics of the chromosphere. Earlier observations showed the increased emission of He I triplet after flares (Penn, M. J. & Kuhn, J. R. (1995), Li et al. (2007), Sasso, C. et al. (2011), Kuckein et al. (2015)). The increased emission was explained to be connected with the bombardment of non-thermal electrons after flares (Nagai, F. & Emslie, A. G. (1984), Tei et al. (2018), Anan et al. (2018)). On the other hand, Si I 10827 Å line, formed in the upper photosphere, showed no significant change in earlier observations. At the same time, some models of flare-related photosphere-chromosphere predicted the increase in its intensity.

To study the behaviour of Si I 10827 Å line, we performed full-Stokes spectro-polarimetric observations during consecutive C-class flares on the GREGOR Infrared Spectrograph. These observations cover spectral interval that includes the photospheric Ca I 10839 Å and Si I 10827 Å lines, with the chromospheric He I 10830 Å triplet line. This paper presents observations of dynamics occurring in the active region in both the photosphere and chromosphere during and after the flare events.

## 2. OBSERVATIONS

On July 16 (2023), we observed a chromospheric dynamic high-speed jet-like structure in the active region NOAA 3363, with accompanying a C4.7 and C3.5 class flares, using the 1.5-$m$ GREGOR telescope (Schmidt et al. (2012)). Spectropolarimetric data were obtained from the GREGOR Infrared Spectrograph (GRIS, Collados et al. (2012)), in conjunction with the High-resolution Fast Imager (HiFI+, Denker et al. (2018b); Denker et al. (2018a); Kuckein et al. (2016); Denker et al. (2023)). The observations were made in spectropolarimetric mode, and the GREGOR polarimetric calibration unit (Hofmann et al. (2012)) was used to carry out the polarimetric calibration of the data. The GREGOR telescope incorporates the GREGOR adaptive optics system (GAOS, Berkefeld et al. (2010)), which operated effectively throughout the observation period under favourable conditions.

The GREGOR Infrared Spectrograph (GRIS, Collados et al. (2012)) captured full-Stokes spectra within the Si I 10827 Å spectral range. Telescope was operated within the 1.0 - 2.3 $\mu m$ range, the spectra most frequently utilized 1.083 $\mu m$, which includes both the photospheric Si I and the chromospheric triplet He I (Collados et al. (2012)). Each step involved eight accumulations, with an exposure time of 100 $ms$ per accumulation. The map consisted of 105 steps, covering approximately ~10 min of observation time. The step size and pixel size along the slit were both 0.135″, resulting in a field of view (FOV) of 60″×15″. In detailed spectral range, they have covered the photospheric lines Ca I 10838.97 Å (deeper photosphere) and Si I 10827.09 Å (upper photosphere), both of which are Zeeman triplets characterized by an influential Landé factor of geff = 1.5 (Balthasar et al. (2016)). Additionally, the spectrum encompassed the chromospheric He I 10830 Å triplet (upper chromosphere), with each spectral sample spaced at intervals of 18 mÅ.

We observed a chromospheric jet-like structure with two consecutive flares of C4.7 and C3.5 classes near the active region NOAA 3363 (X: 728″, Y: −346″) on July 16, 2023 (Figure 1). During the peak of the first flare at 08:41 UT, the GREGOR slit location, denoted by the red rectangle in Figure 1, was positioned over the active region NOAA 3363. This positioning allowed for targeted observations of specific solar features crucial for understanding jet dynamics. The accompanying C4.7 class flare started at 08:31 UT, peaked around 08:41 UT and ended at 08:45 UT. Subsequently, the consecutive C3.5 class flare began at 08:46 UT, peaked around 08:50 UT, and ended at 08:56 UT(Figure 1 lower right panel). The observations consisted of spatial scans performed during specific phases of these flares: the first scan was performed during 08:41 UT - 08:44 UT, with the corresponding chromospheric jet flying toward the sunspot(Figure 2 white arrow) after C4.7 class flare peak. The second scan was performed from 08:44 UT - 08:47 UT, corresponding to the declining phase of the C4.7, and the third scan was performed from 08:47 UT - 08:50 UT, corresponding to the initial phase of C3.5. Additionally, an extra scan of the same area was conducted immediately after the third scan, which covered the time from 08:51 UT to 08:58 UT (peak and declining phase of the C3.5 flare). Exciting and spectacular profiles were observed during the third scan(Figure 1 and Figure 3 red and blue asterisk.) Hence, the data covered almost the entire duration of the two flares. By aligning the GREGOR slit with the active region and utilizing multiple imaging modalities, including magnetograms and multi-wavelength observations, our study aims to capture the complex interplay between magnetic field reconnection and solar dynamics during the event. These observations provide a comprehensive dataset for analyzing the evolution of the dynamic Jet-like structure and its impact on the solar atmosphere across different layers and wavelengths.

### 2.1. Data preparation
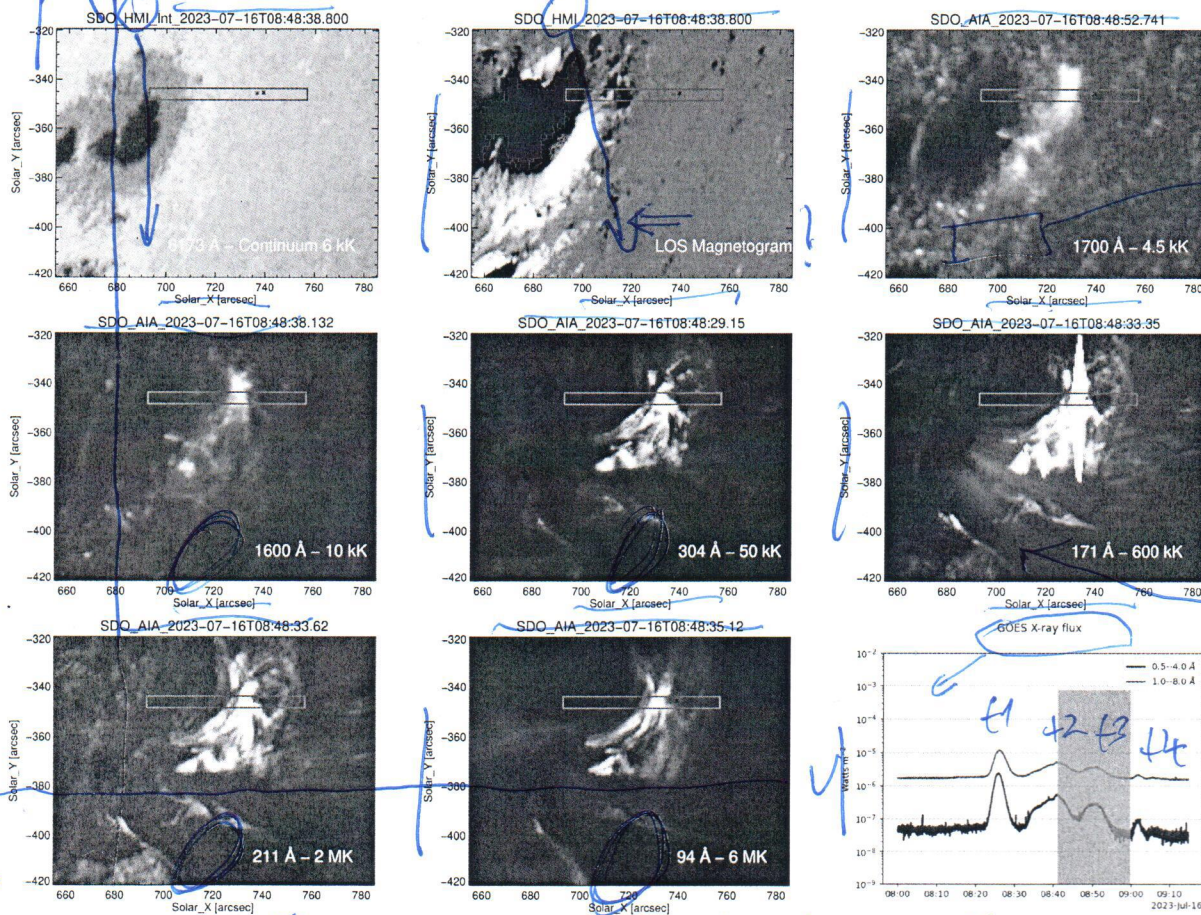
**Figure 1.** GREGOR Slit location (red rectangle) on SDO HMI-AIA images during the flare initiation at 08:48 UT and Time evolution of the X-ray flux in GOES satellite channel 1.0 - 8.0 Å (red) and 0.5 - 4.0 Å (blue). On the upper left and middle panel, the active region NOAA 3363 is present in the SDO/HMI Magnetogram images. The SDO/AIA image of the Photosphere/Chromosphere region(1700 Å) is shown on the right upper panel. The Upper Photosphere/Transition region(1600 Å), the Transition region/Chromosphere (304 Å) and the Quiet corona/upper transition region(171 Å) are shown on the middle panels, respectively(from left to right). SDO/AIA images of the active region(211 Å) and Flare region(94 Å) were shown on the lower right and middle panels. On the lower right panel: X-ray flux for 08:00 UT-09:10 UT of 2016-07-16 and with the grey rectangle marked the observed time of C4.7 and C3.5 class flare in NOAA 3363 active region. Red and blue asterisks mark locations where spectacular profiles are observed.

Data processing has been performed according to typical steps of observations on the GREGOR telescope. The process includes photometric corrections, dark current subtraction, flat fielding, and polarimetric-calibration and cross-talk removal according to the standard GRIS data reduction software, as described by Collados (1999); Collados (2003). The data underwent dark and flat-field correction, as well as polarization calibration using the GREGOR polarimetric unit (Hofmann et al. (2012)) and standard procedures outlined by Collados (Collados (1999); Collados (2003)). Following calibration, the Stokes profiles were normalized to the average continuum level, calculated from various areas across the field of view (FOV), with regions displaying significant polarization signals excluded from the analysis.

After the mentioned corrections, additional adjustments were needed. The useful tool is Cassda GUI, a program developed by the Kiepenheuer-Institut für Sonnenphysik for data preparation. [1] The software automatically removed

[1] https://gitlab.leibniz-kis.de/sdc/gris/cassda_gui

Ca I 10838.97 A line core 08:41:26–08:43:54

Si I 10827.1 A line core 08:41:26–08:43:54

He I 10829.09 (+0.2A) 08:41:26–08:43:54

Stokes I 08:42:26UT

Stokes V 08:42:26UT

Ca I

tell.

Si I   He I
tell.

(36.86",3.92")
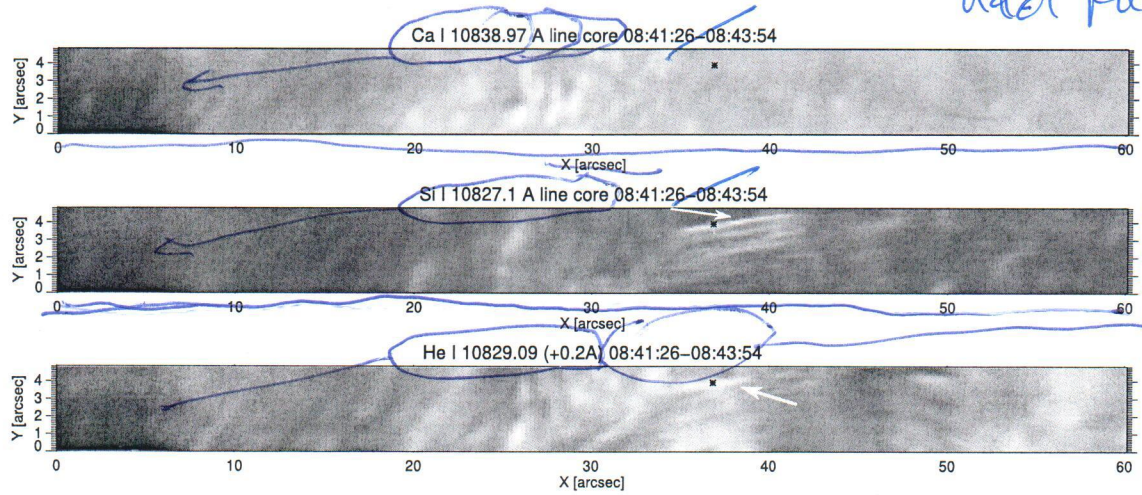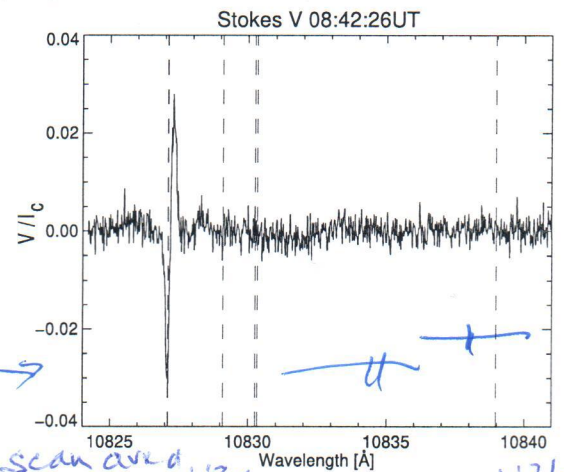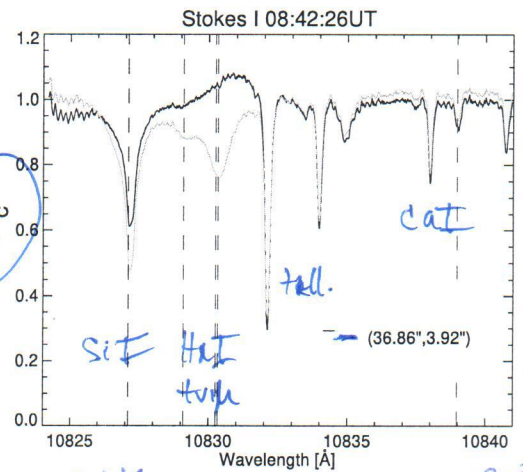
**Figure 2.** First - third row: Full GREGOR/GRIS slit in Ca I 10839 Å (upper panel), Si I 10827 Å (middle panel) and He I 10830 Å triplet red wing of "blue" component (below panel) during the observation time 08:41:26-08:43:54 UT. A white arrow shows a high-speed chromospheric jet. A black asterisk showing the position of the Stokes profile is presented on the fourth row. The spectral interval covered the following lines (from left to right): Si I line, He I triplet, two telluric lines and Ca I line. Vertical dashed lines indicate the static wavelengths of the Si I 10827.09 Å line (blue), the He I triplet (red), and Ca I 10838.97 Å (purple) respectively. For comparison, the average quiet-sun intensity spectrum is presented as an orange line on the Stokes I profile.

the spikes using the interpolation method. The spectrograph still exhibited continuum intensity variations that required correction. To address this and for wavelength calibration, we utilize the IAG spectral atlas obtained with the Fourier Transform Spectrograph (Reiners, A. et al. (2016)). The continuum correction curve is derived by fitting a polynomial to the ratio of the disk centre slope from our observations and the slope of the atlas spectrum. Telluric lines in the observed spectral region are utilized for wavelength calibration. The calculated spectral dispersion is 18 mÅ per pixel. Finally, the observed spectrum is normalized to the continuum level of the quiet Sun at the disk centre, a step necessary for the inversions.

In this study, our emphasis is on the derived magnetic field strength and line-of-sight velocity patterns.

## 3. DATA ANALYSIS

To deduce the flare's magnetic field configuration and thermodynamic parameters, we utilize the Hazel inversion code (Ramos et al. (2008)) to fit the profiles of He I 10830 Å and Si I 10827 Å. In addition, the photospheric Si I line was analyzed using the Weak Field Approximation. The HAZEL (HAnle and ZEeman Light; ?) inversion code was employed to determine the chromospheric magnetic field vector from the observations. This code necessitates
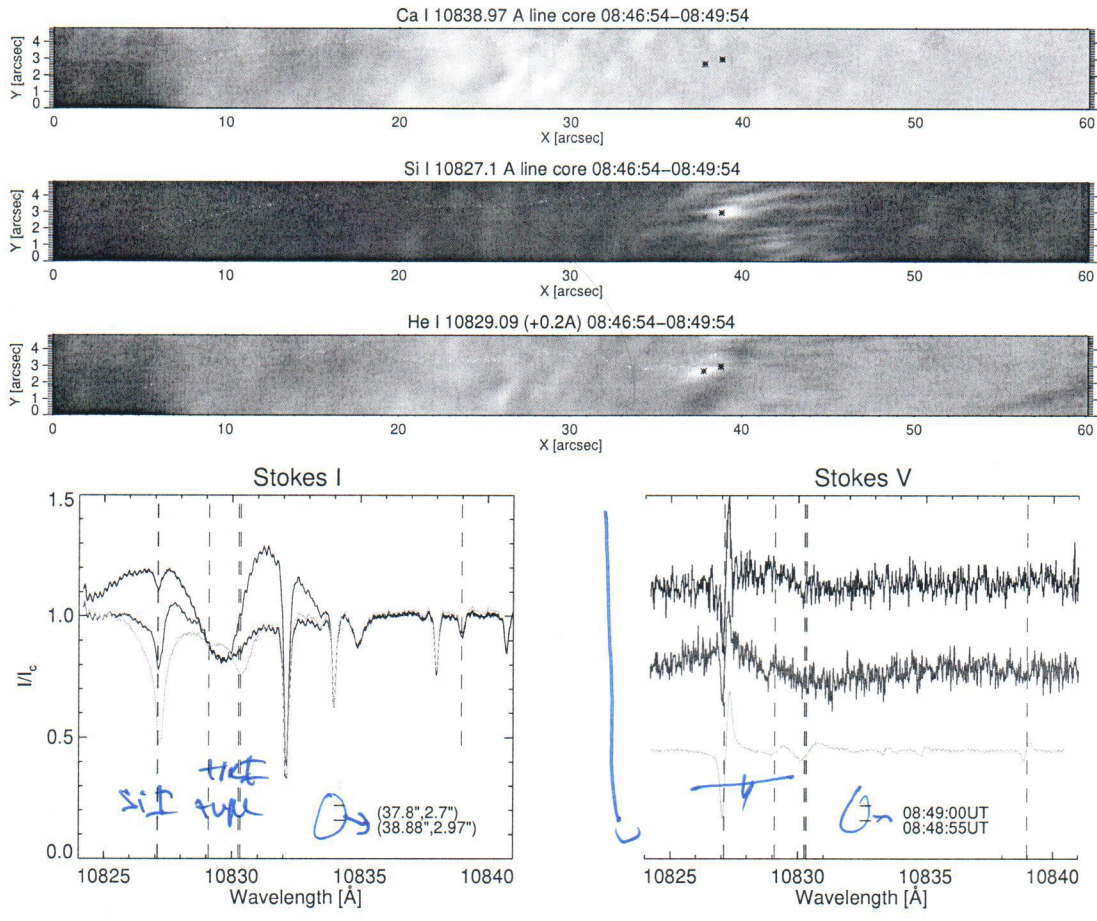
**Figure 3.** Full GREGOR/GRIS slit in Ca I 10839 Å (first row), Si I 10827 Å (middle row) and He I 10830 Å triplet red wing of "red" component (third row) during the observation time 08:46:54-08:49:54 UT. Normalized Stokes I profiles at different locations, indicated by the different colours (Left Panel of the fourth row). Orange colour: quiet sun profile, red: He I redshifted emission profile, and blue: profile indicating strongly blueshifted He I line, profiles are from different locations (red and blue asterisk first - third rows). Stokes V profiles corresponding to Stokes I profiles are presented in the left panel of the last row. Not to overplot Stokes V profiles; they are placed separately beside each other. Vertical dashed lines indicate the static wavelengths of the Si I 10827.09 Å line (blue), the He I triplet (red), and Ca I 10838.97 Å (purple) respectively.

the full Stokes vector data, the observation angle, and an initial estimate as inputs. The code considers atomic level polarisation and Zeeman, Hanle, and Paschen-Back effects. The model assumes a slab for the upper photosphere, silicone, and three slabs with constant properties that are asymmetrically illuminated from below and in the telluric line. The irradiation of the slab accounts for the center-to-limb variation. We used the code in the mode of a single optically thick slab. These slabs are positioned at a height h above the solar surface and are subjected to a deterministic magnetic field with arbitrary strength, inclination, and azimuth. We allowed high up-flow velocities. The SIR inversion code utilizes response functions to solve the radiative transfer equation, assuming local thermodynamic and hydrostatic equilibrium.

The inversion code determines various physical parameters, including the magnetic field vector components, temperature, and Doppler velocity. We constrained the inversions to a single node for Doppler velocity, magnetic field strength, inclination, and azimuth, maintaining these values as constant with height. Conversely, the temperature varies with height, employing one, three, and four nodes in the different stages of SIR. We consistently set the macroturbulence to 750 $m\ s^{-1}$ throughout the entire inversion process without any alterations. The GRIS spectropolarimeter allows us to study the chromosphere through the He I 10830 Å line produced in the chromosphere. We used the Hanle and Zeeman Light (HAZEL) code to invert the Stokes parameters of the helium triplet.

## 4. RESULTS

Figure 2 shows the first scan of selected AR in Ca I 10839 Å (Fig. 2 first row), Si I 10827 Å (Figure 2 middle row) and He I 10830 Å triplet(Fig. 2 third row). The spectral line position for Ca,I and Si I was selected at the line core. But for the He I triplet, the red wing of the "blue" component of the line was selected. The chromospheric high-speed jet-like structure is seen in both Si I and He I spectral lines(Figure 2 white arrow). Figure 2 black asterisc showing the normalized Stokes profiles (black lines) at 08:42 UT (Fig.2 fourth row), corresponding to the point from the jet-like structure after the peak of the first flare. The orange line on Stokes I denotes the average quiet-sun intensity spectrum.
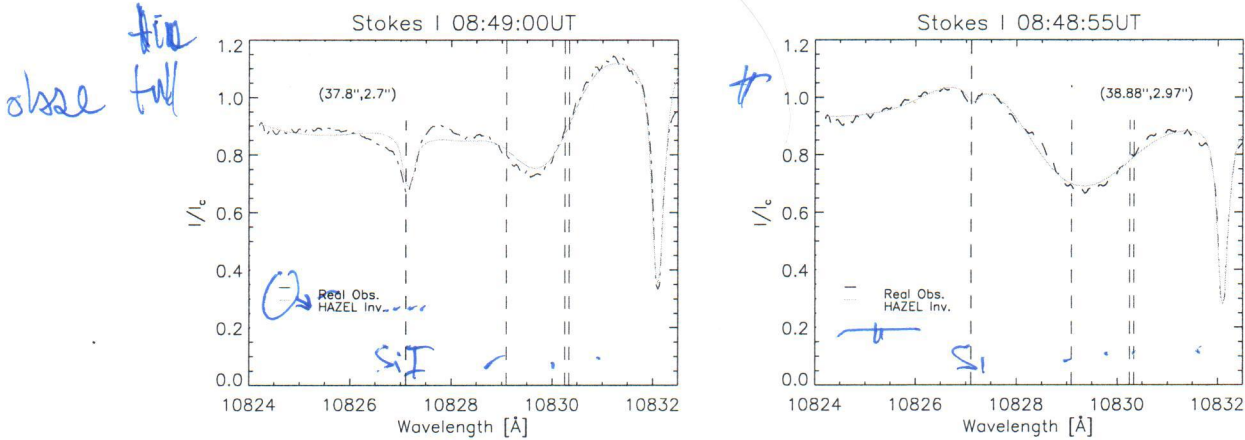


**Figure 4.** Example of Observed Emission Stokes I profiles (red, blue) and HAZEL inverted profiles (orange) of He I and Si I lines during the post-phase of C4.7 flare and the pre-phase of C3.5 flare. The left panel presented He I redshifted emission profile (Fig.3 red coloured profile), and the right panel shows a strongly blueshifted He I line, with modified Si I line (Fig.3 blue coloured).

It is seen that the He I triplet is transformed from absorption to emission behaviour accompanied by significant redshift. The He I 10830 Å triplet line originates in the upper chromosphere. Therefore, the increase in emission is probably related to the upflow jet-like structure shown by the white arrow in Figure 2 or, on the other hand, increased temperature in the chromosphere after a flare. The increased emission of He I triplet with regards to the continuum during flares has been continuously reported, ~1.36 times during M2.0 flare (Li et al. (2007)), ~1.30 times during the decay phase of a C9.7 flare (Penn, M. J. & Kuhn, J. R. (1995)), and ~1.15 during a C2.0 flare (Sasso, C. et al. (2011)). Kuckein et al. (2015) observed maximal increase of He I 10830 Å line emission by ~1.86 with the red component. In our case, the red component of He I Stokes I profile reached the emission ratio of ~1.1 just after the C4.7 flare all over across the jet from 08:42:05 UT - till 08:42:42 UT. The jet-like structure has a ~ 5″ length and a velocity of ~ 95 $km\ s^{-1}$.

Figure 3 also shows the normalized Stokes profiles from different locations and times, corresponding to an example of the unusually wide range of Stokes profiles observed. The Stokes red-coloured profiles were taken at the spatial location indicated by the red asterisk in Figure 1 and Figure3. The orange line represents a profile observed in a quiet sun region during our observations (Fig. 3 fourth row). The black colour line spectrum shows a He I line in emission and redshifted 7 min later after the C4.7 flare maximum, at 08:49 UT and showed a peak at ~1.3 (Fig. 3 fourth row). The blue colour Stokes I shows strongly blueshifted of He I line at 08:48:55 UT. The blueshift is so large that it reaches even the blue wing of the Si I line at 10827.1 Å, corresponding to ~ 90 $km\ s^{-1}$. The above rows in Figure 3 show the full GREGOR/Gris slit and locations of the redshifted(red asterisk Fig.3) and blueshifted(blue asterisk Fig.3) Stokes profiles. Observed Stokes V profiles are plotted next to each other for a better view (Fig. 3, right panel of the last row).

Figures 2 and 3 show no significant change in Ca I 10839 Å (First row and Purple vertical dashed line on Stokes profiles panels). It is suggested that the increase of He I 10830 Å emission is due to the bombardment of non-thermal electrons after flares (Anan et al. (2018)). The non-thermal electrons penetrate in the chromosphere to the depth according to their kinetic energy and the surrounding density, where they deposit the energy and increase the plasma
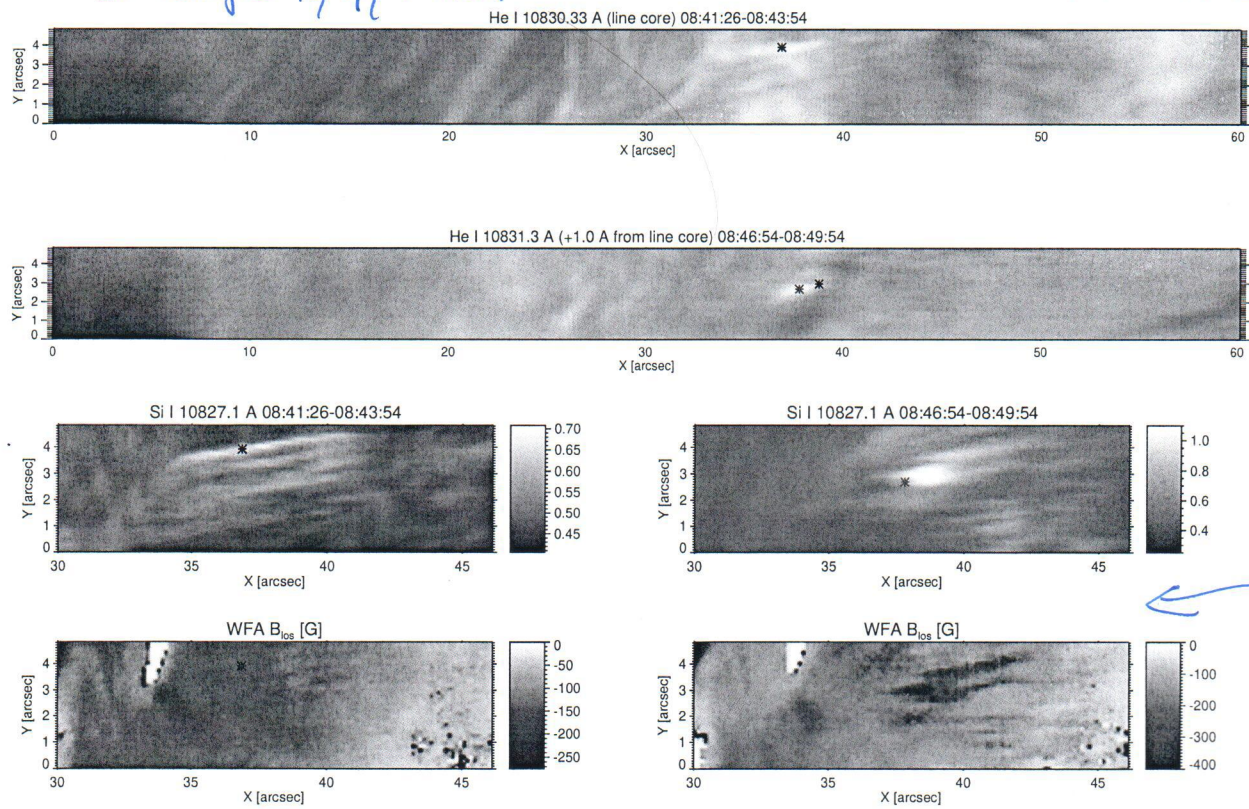
temperature significantly (Nagai, F. & Emslie, A. G. (1984); Tei et al. (2018)). As the electrons lose the energy, they do not penetrate in the photosphere, where Ca I 10839 Å line is formed. Hence, the line is not affected. However, Figure 3 shows a significant change in Si I 10827 Å line, mostly because of the large blueshift of He I line.



**Figure 5.** First row: Full slit in He I 10830 Å line during the observation time 08:41:26-08:43:54 UT, with black asterisk showing the position of the Stokes profiles in Fig.2. Second row: The He I 10830 Å line red wind (+1.0Å) during the observation time 08:46:54-08:49:54 UT, with blue and red asterisks showing the position of the Stokes profiles in Fig.3. Third row: Slit-reconstructed monochromatic intensity images of Si I line (left and right panel). Fourth row: magnetic field **B** in Si I spectral line.

Figure 4 shows the observed Stokes I (black colour) and HAZEL inverted (orange) profiles at different times corresponding to the third scan. The left column corresponds to the place marked with a red asterisk in Figure 1 and Figure 3. The right column shows the spectra from the place marked with a blue asterisk in Figure 3. The profiles show interesting behaviour of spectral lines. Ca I 10839 Å line shows no significant change during the event. But the profile of Si I significantly increases in intensity. The line core still shows absorption, but the wings are dominated by emission, which indicates a significant increase in plasma temperature of the upper photosphere, where the line is formed. This figure delineates the temporal sequence from the aftermath of the C4.7 class flare to the intro of the ensuing C3.5 class flare. HAZEL inversion show the significant supersonic downflow and up-flow with $\pm 90 - 150$ $km$ $s^{-1}$ LOS velocity range. The depiction in the left panel of Figure 4 is of particular interest, which presents the observed profile of Si I, revealing an unexpected emission feature or strong blueshifted He I line. Traditionally, Si I is recognized as primarily an absorption line; however, the manifestation of emission in this context signifies a significant perturbation in temperature after the flare event and the subsequent emission of He I 10830 Å. Thus, the discerned alterations in the Si I profile denote a pronounced shift in thermal conditions during the post-flare phase.

Figure 5 shows the full slit in He I 10830.33 Å line core during the observation time 08:41:26-08:43:54 UT(first-row) and the line red wing (+1.0Å) at time 08:46:54-08:49:54 UT(second-row). The black and red asterisks show the position

center intensity ←

of the same colour Stokes profiles in Figure 2 and Figure 3. Slit-reconstructed monochromatic intensity images of Si I line (left and right panel) on the third row of Figure 5. These images precisely capture the portion of the entire scanned field of view corresponding to the post-flare phase of the C4.7 class flare and the pre-flare phase of the subsequent C3.5 class flare.

Fig. X! ADD

A clear increase of intensity in Si I and He I lines are seen during the third scan, corresponding to the second flare's rising phase. We performed the Weak Field Approximation of Si I 10828 Å line. It has a relatively low Landé factor ($g_{eff} = 1.5$) and a strong magnetic field. The resulting upper photospheric magnetic field strength is shown in Figure 5, fourth row. In Figure 5 we present a jet-like structure during the post-flare phase of the C4.7(left panel) and redshifted emission of the He I line during the pre-flare phase of the C3.5 class flare(right panel). With a small time difference of $\sim 5$ s and a short distance apart, the He I line blueshift is shown in the second row of Figure 5 (blue asterisk). Which representation of the supersonic downflows in the chromosphere, connected to He I 10830.33 Å loops. These downflows are found along the loops and at their footpoints, with velocities increasing towards the footpoints (Sowmya, K. et al. (2022)). At approximately 8000–10,000 $K$ formation temperature for the He I 10830 Å triplet, the sound speed is around 10 $Km\ s^{-1}$. The observed average velocities of the magnetized supersonic downflows range from 1.5 to 2.7 times the local sound speed, consistent with the values reported by Manrique et al. (2020). In a flaring active region filament, Sasso, C. et al. (2011) recorded redshifts reaching up to 100 $km\ s^{-1}$. However, in the active regions, they analyzed, none flared during their observations, and downflows did not exceed 50 $Km\ s^{-1}$. In our case, the downflows speed reaches $\sim 150 Km\ s^{-1}$.

STOP READING

6.

## 5. DISCUSSION AND CONCLUSION

Several scenarios have been proposed in the literature to explain the origin of highly redshifted and blueshifted flows. The downflows in loops or arch filament systems (AFSs) are typically interpreted as the result of plasma draining from emerging flux tubes (Chou, D. Y. (????); Solanki S. K. et al. (2003); Lagg, A. et al. (2007); Xu et al. (2010); Balthasar et al. (2016); González Manrique, S. J. et al. (2018)). Upflows with subsonic velocities are observed at the loop tops for the slow component, while faster downflows are detected closer to the footpoints, indicating gravitational acceleration of the material as it descends along the loop. Our observations show a distinctly redshifted emission representing a chromospheric jet-like structure in Figure 2(white arrow). The blueshifted absorption of the He I 10830 Å line (Fig. 3 blue asterisk) represents the supersonic downflow connected to He I 10830.33 Å loop(Fig.1, Fig.3 and Fig. 5 blue asterisk).

GOING UP OR DOWN.

BLUE DOWNFLOW?

Presented slit scan and spectrum of the infrared spectral region around He I 10830 Å including photospheric Ca I 10839 Å line and upper photospheric Si I 10827 Å line, conducted during the high-speed chromospheric jet accompanied with C4.7 and C3.5 class flares. Observations were performed using the Infrared Spectrograph GRIS. As expected, Ca I 10839 Å line are not changed during the flare events. Upper chromospheric He I 10830 Å triplet line shows the increase of intensity all over the jet-like structure, starting from the post-flare phase of the C4.7 class flare. The intensity of the upper photospheric Si I line starts to increase in $\sim 7$ min after the increase of He I 10830 Å line intensity. This means that the upper photosphere, where the Si I line is formed, is heated after several minutes of upper chromospheric heating.

The upper chromospheric heating, which results in the intensity enhancement of He I 10830 Å line, is caused by the high-speed, dynamic jet-like structure releasing high-energy electrons. But the mechanism for heating the upper photosphere, which results in the intensity enhancement of Si I line, is unclear. Heating due to the electrons can be excluded because of the jet-like structure, mostly up-flow injection. On the other hand, heat transportation may be due to thermal conduction. The distance from the upper chromosphere to the upper photosphere is $\sim 1500$ km, yielding a communication speed of 5 $Km\ s^{-1}$. This speed is close to the speed of thermal conduction rather than the velocity of flare-induced electrons. As expected, the temperature of the lower photosphere did not significantly increase after the flare.

## REFERENCES

Anan, T., Yoneya, T., Ichimoto, K., et al. 2018, Publications of the Astronomical Society of Japan, 70, 101, doi: 10.1093/pasj/psy105

Balthasar, H., Gömöry, P., González Manrique, S. J., et al. 2016, Astronomische Nachrichten, 337, 1050, doi: 10.1002/asna.201612432

Beckers, J. M. 1968, Solar Physics, doi: 10.1007/BF00171614

Berkefeld, T., Soltau, D., Schmidt, D., & von der Lühe, O. 2010, Appl. Opt., 49, G155, doi: 10.1364/AO.49.00G155

Chou, D. Y. ????, 46

Collados, M. 1999, in Astronomical Society of the Pacific Conference Series, Vol. 184, Third Advances in Solar Physics Euroconference: Magnetic Fields and Oscillations, ed. B. Schmieder, A. Hofmann, & J. Staude, 3–22

Collados, M., López, R., Páez, E., et al. 2012, Astronomische Nachrichten, 333, 872, doi: 10.1002/asna.201211738

Collados, M. V. 2003, in Polarimetry in Astronomy, ed. S. Fineschi, Vol. 4843, International Society for Optics and Photonics (SPIE), 55 – 65, doi: 10.1117/12.459370

De Pontieu, B., McIntosh, S., Hansteen, V. H., et al. 2007, Publications of the Astronomical Society of Japan, 59, S655, doi: 10.1093/pasj/59.sp3.S655

Denker, C., Kuckein, C., Verma, M., et al. 2018a, The Astrophys. J. Supplement Series, 236, 5, doi: 10.3847/1538-4365/aab773

Denker, C. J., Dineva, E., Balthasar, H., et al. 2018b, Solar Physics, 293, 44, doi: 10.1007/s11207-018-1261-1

Denker, C. J., Verma, M., Wiśniewska, A., et al. 2023, Journal of Astronomical Telescopes, Instruments, and Systems, 9, 015001, doi: 10.1117/1.JATIS.9.1.015001

González Manrique, S. J., Kuckein, C., Collados, M., et al. 2018, AA, 617, A55, doi: 10.1051/0004-6361/201832684

Hofmann, A., Arlt, K., Balthasar, H., et al. 2012, Astronomische Nachrichten, 333, 854, doi: https://doi.org/10.1002/asna.201211733

Kuckein, C., Collados, M., & Sainz, R. M. 2015, The Astrophys. J. Letters, 799, L25, doi: 10.1088/2041-8205/799/2/L25

Kuckein, C., Denker, C., Verma, M., et al. 2016, Proceedings of the International Astronomical Union, 12, 20

Lagg, A., Woch, J., Solanki, S. K., & Krupp, N. 2007, AA, 462, 1147, doi: 10.1051/0004-6361:20054700

Li, H., You, J., Yu, X., & Du, Q. 2007, Solar Physics, 241, 301, doi: 10.1007/s11207-007-0282-y

Manrique, S. J. G., Kuckein, C., Yabar, A. P., et al. 2020, The Astrophysical Journal, 890, 82, doi: 10.3847/1538-4357/ab6cee

Moore, R. L., Sterling, A. C., Cirtain, J. W., & Falconer, D. A. 2011, The Astrophysical Journal Letters, 731, L18, doi: 10.1088/2041-8205/731/1/L18

Nagai, F., & Emslie, A. G. 1984, The Astrophys. J., 279, 896, doi: 10.1086/161960

Penn, M. J., & Kuhn, J. R. 1995, The Astrophys. J. Letters, 441, 51, doi: 10.1086/187787

Ramos, A. A., Bueno, J. T., & Degl'Innocenti, E. L. 2008, The Astrophysical Journal, 683, 542, doi: 10.1086/589433

Reiners, A., Lemke, U., Bauer, F., Beeck, B., & Huke, P. 2016, A&A, 595, A26, doi: 10.1051/0004-6361/201629088

Roy, J. R. 1973, Solar Physics, 28, 95, doi: 10.1007/BF00152915

Sasso, C., Lagg, A., & Solanki, S. K. 2011, A&A, 526, A42, doi: 10.1051/0004-6361/200912956

Schmidt, W., von der Lühe, O., Volkmer, R., et al. 2012, Astronomische Nachrichten, 333, 796, doi: 10.1002/asna.201211725

Shibata, K., Nakamura, T., Matsumoto, T., et al. 2007, Science, 318, 1591, doi: 10.1126/science.1146708

Solanki S. K., Lagg A., Woch J., Krupp N., & Collados M. 2003, Nature, 425, 692–695, doi: 10.1038/nature02035

Sowmya, K., Lagg, A., Solanki, S. K., & Castellanos Durán, J. S. 2022, AA, 661, A122, doi: 10.1051/0004-6361/202142850

Sterling, A. C., Moore, R. L., Samanta, T., & Yurchyshyn, V. 2020, The Astrophysical Journal Letters, 893, L45, doi: 10.3847/2041-8213/ab86a5

Tei, A., Sakaue, T., Okamoto, T. J., et al. 2018, Publications of the Astronomical Society of Japan, 70, 100, doi: 10.1093/pasj/psy047

Tsiropoula, G. Tziotziou, K. K. I. M. M. S. D. J. G., & Suematsu, Y. 2012, Space Science Reviews, 169, 181, doi: 10.1007/s11214-012-9920-2

van der Voort, L. R., Leenaarts, J., de Pontieu, B., Carlsson, M., & Vissers, G. 2009, The Astrophysical Journal, 705, 272, doi: 10.1088/0004-637X/705/1/272

Xu, Z., Lagg, A., & Solanki, S. K. 2010, A&A, 520, A77, doi: 10.1051/0004-6361/200913227

Yoshimura, K., Kurokawa, H., Shimojo, M., & Shine, R. 2003, Publications of the Astronomical Society of Japan, 55, 313, doi: 10.1093/pasj/55.1.313